



Dynamic Monitoring of Polymer Flooding Using Magnetic Resonance Imaging Technology

Hongxian Liu¹ · Yao Ding² · Weimin Wang²  · Yingkang Ma² · Taotao Zhu² · Deming Ma²

Received: 8 June 2020 / Revised: 9 September 2020 / Accepted: 30 September 2020 /

Published online: 17 October 2020

© Springer-Verlag GmbH Austria, part of Springer Nature 2020

Abstract

Polymer flooding is a vital method for the enhanced oil recovery of heterogeneous formations after water flooding. However, few visualization approaches are available to conduct the online monitoring and the non-invasive evaluation of polymer flooding experiments in natural rock cores. In this study, online dynamic magnetic resonance imaging (MRI) and T_2 distribution measurements were employed to monitor polymer flooding in a natural layered core using low-field MRI equipment. A modified spin echo (SE) imaging technique featuring half Fourier acquisition and a short echo time (3.5 ms) was used to achieve dynamic MRI images during flooding with a temporal resolution of 93 s. Moreover, online T_2 distribution measurements by the Carr-Purcell-Meiboom-Gill (CPMG) pulse sequence were utilized to estimate the bulk remaining oil saturation to validate the MRI results. Furthermore, the spatial distribution of the displacement efficiency was obtained through MRI signal processing and was visualized via a pseudo-colour mapping technique. A statistical analysis was carried out to estimate the change in the mean of the spatial distribution of the displacement efficiency. The results show that an improvement in the oil recovery from the natural layered core by polymer flooding after water flooding can be intuitively observed by the proposed method. Our low-field MRI methods provide quantitative and revealing information that can be beneficial for flooding mechanism studies of enhanced oil recovery.

Hongxian Liu and Yao Ding the authors have the same contribution.

✉ Weimin Wang
wmw@pku.edu.cn

¹ Faculty of Petroleum, China University of Petroleum–Beijing at Karamay, Karamay 834000, China

² Department of Electronics, Peking University, Beijing 100871, China

1 Introduction

Polymer flooding is an economical enhanced oil recovery method for heterogeneous reservoirs that is utilized after water flooding. It is generally accepted that the main recovery mechanism of polymers is to increase the water phase viscosity and decrease the water relative permeability due to polymer retention so that volumetric sweeps are improved by mobility reduction [1, 2]. In addition, the viscoelastic properties of polymers also have a certain role in improving the microscopic oil displacement efficiency [3–5].

Core flooding experiments are typically used to determine the optimal reservoir development option and to evaluate the effects of injected fluids that are specially designed to improve or enhance oil recovery [6, 7]. In conventional experiments, the core plug is generally regarded as a black box, and the bulk oil saturation and oil recovery rate of the core are estimated by the inlet and outlet dynamics [8, 9]. It is well known that recovered fluids are probably emulsified [10]; moreover, a small amount of effluent makes accurate measurements difficult to achieve, resulting in a large deviation in the calculation. The spatial distribution of the oil saturation or sweep efficiency in the core plug is difficult to obtain through traditional flooding experiments [7].

Low-field nuclear magnetic resonance (LFNMR) technology has become a powerful tool for logging and laboratory core analysis with advantages of low cost, simple maintenance, and a low induced internal field gradient in the pores [11–14]. This method mainly relies on the CPMG sequence [15, 16] to measure the T_2 decay signal. Through the inversion of this time domain signal, the T_2 distribution can be obtained, and the porosity, permeability, pore size distribution, and movable fluid saturation can be quantitatively estimated. To improve the capability of fluid typing, researchers have developed a two-dimensional correlative spectrum (DT_2 , T_1T_2) and corresponding regularized inversion methods based on data compression [17–20]. Because the NMR detection signal is strictly proportional to the hydrogen content in samples, it offers a fast and non-destructive way to measure the fluid content. Moreover, this method not only provides the relaxation time in the statistical domain, indicating the state of the fluid occurrence by which the pore size distribution and wettability could be inferred, but also provides the imaging function of MRI to give the spatial information of the fluid confined in the core; this technology is considered to have the most potential for core analysis.

We built an MRI compatible flooding system in a 0.35 T low-field MRI imaging system. A modified spin echo (SE) imaging technique featuring half Fourier acquisition and a short echo time (TE, 3.5 ms) was used to achieve dynamic MRI imaging of the core plug during the flooding process with a temporal resolution of 93 s. In addition, the system also conducted traditional T_2 distribution measurements at the same time, which facilitated an estimation of the bulk remaining oil saturation to validate the MRI method. A natural layered core plug in the Xinjiang oilfield was studied by online NMR dynamic imaging and T_2 -distribution measurements during the polymer flooding process. A kinetic low-field image array was obtained, and the flooding process was analysed in detail.

2 Method

2.1 T2 Distribution

Spins precess at Larmor frequencies when they are placed in the main magnetic field (B_0). The ensemble of spins exhibits net magnetization (M) in the equilibrium state, aligned with the direction of B_0 . When stimulated by radio frequency (RF) pulses, M is rotated to an angle (typically 90° or 180°) that depends on the duration of the pulse. As the RF pulse ceases, M will relax towards and reach the equilibrium state. The recovery process is called relaxation, during which T_1 and T_2 are used as time constants to reflect the changing speed of the longitudinal component and transverse component of the magnetization vectors, respectively. Because of the fast measurement speeds of T_2 distribution via the “one shot” CPMG pulse sequence, T_2 distributions is widely used in logging and laboratory core analysis rather than T_1 distribution. Despite that T_1 is not affected by apparent relaxation due to diffusion in internal gradients, routine T_1 measurement via inversion recovery or saturation recovery is much longer than T_2 measurement.

The transverse relaxation mechanism of fluid confined in rock pores consists of three types: bulk relaxation, surface relaxation and apparent relaxation due to diffusion in internal gradients [11–13, 21]. In the case of a fast diffusion regime [22], the surface relaxation rate ($1/T_{2s}$) is equal to the surface relaxivity multiplied by the surface to volume ratio (S/V). In general, the surface relaxation of brine is much stronger than the bulk relaxation, and the apparent relaxation due to diffusion can be neglected with short inter-echo spacing under low-field conditions. Therefore, the apparent relaxation time corresponds well with the pore size when saturated with brine. Since rock is composed of pores of different sizes and each pore has its own characteristic relaxation time, the NMR response of the fluid confined in the rock core behaves multi-exponentially. The multi-exponential attenuation (CPMG decay signal) is described by a set of relaxation time constants, and their signal magnitude is associated with each T_2 constant, which is called the T_2 distribution.

2.2 Imaging Method

The precession frequency of spins is equal to the product of the gyromagnetic ratio and the magnetic field strength. The x, y, and z gradient coils provide an additional constant gradient on the main magnetic field in their respective directions, so the spatial precession frequencies of spins are different, which allows spatial encoding. Generally, slice selection, frequency coding, and phase coding are performed to achieve magnetic resonance imaging [23].

Pure phase encoding MRI was reviewed by Muir [24]. This method is effective in one-dimensional (1D) saturation profile determination [25] and static sample imaging [26, 27], enabling the imaging of materials characterized by dramatically shorter T_2 relaxation times. However, due to its long acquisition time [26, 27], this technique is almost impractical for imaging dynamic flooding processes, although it is

more suitable for quantitative MRI [28]. Turbo Spin Echo sequence including 3D FSE, π -EPI (based on CPMG spin echo train) were studied by Li and Xiao [29] to monitor dynamic oil displacement processes and exciting results are present with a temporal resolution of 8.3 and 16.6 min respectively. Apparently, the long image time is not suitable for normal displacement flow rate. Because each-line of the K space in these sequences has different T2 weighted, these type images obtained are not pure T2-weighted image. Of course, image quality degradation and serious artifacts are easy to appear owing to induced gradient eddy by frequent switching of phase encoding gradients, so these pulse sequences have high requirements for gradient system to realize precise control of the gradient for good quality spatial encoding. 2D SE image is a good choice for practical enhanced oil recovery experiment for core plug with high permeability. Firstly, reduction of imaging dimensions could reduce imaging time. Secondly, due to filling only one line of K space during each repetition time, each line data has the same relaxation weight. It is more convenient to post-process SE images to get some quantitative information.

The conventional SE pulse sequence method utilizes frequency encoding for rapid k-space filling in one shot. However, due to the long TE of conventional SE imaging, the signal attenuation of the short relaxation component is severe, and the signal-to-noise ratio (SNR) is low, leading to poor imaging quality. Additionally, SE MRI is a T1- or T2-weighted imaging technique that does not provide quantitative information [24, 25]. Therefore, SE technology should be modified to detect short relaxation signals as much as possible, and an appropriate analysis method should be established to obtain quantitative information on rock cores through T1- or T2-weighted images. For the above reason, the refocusing pulse employed a short nonselective 180° hard pulse [30], and a strong read gradient was used to shorten the sampling time. A slice gradient was not applied, and only the 2D projection MRI image in the XY plane was obtained to significantly shorten the TE and greatly relieve the attenuation of the signal. Moreover, since the k-space data have conjugate symmetry and some of the information in the k-space is redundant [31], to further shorten the imaging time and achieve online fast imaging, a half Fourier acquisition method is adopted, and k-space filling is conducted before the Fourier transformation to obtain the images. Although it is called a half scan, it is generally necessary to collect several rows of the centre of the k-space to correct the phase [32]. The timing diagram for the modified SE imaging pulse sequence is shown in Fig. 1. A schematic of the orientation of the core plug is shown in Fig. 2(a). The main magnetic field B_0 is aligned along the z-axis, and the RF B_1 field is applied in the x–y plane. Figure 2b shows the obtained 2D projection imaging without a slice selective gradient.

2.3 MRI Quantitative Characterization

As Sect. 2.2 mentioned, the SE imaging method is T1- and T2-weighted and couldn't directly get a quantitative image to reflect fluid content. However, we could get some quantitative information through comparing relaxation time weighted images. When a core plug in irreducible water sate (initial oil saturation) is flood by injectant in which the water phase is D_2O brine and only the oil

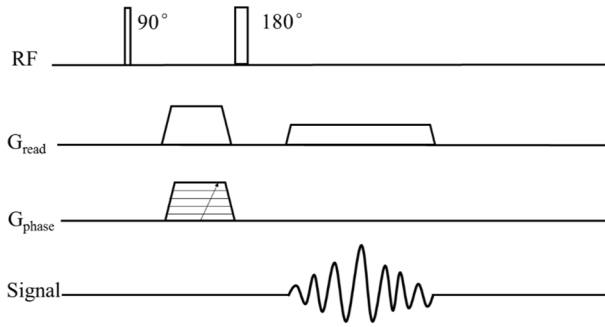


Fig. 1 The timing diagram for the modified spin echo imaging pulse sequence with half Fourier acquisition

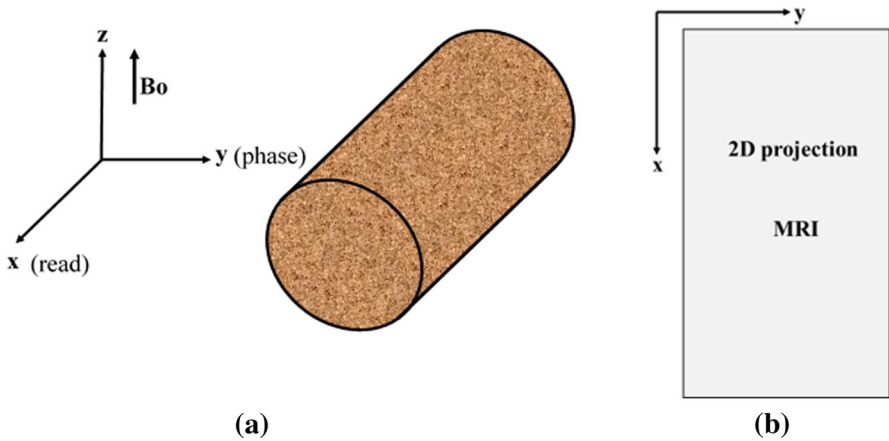


Fig. 2 Schematic of **a** the orientation of the core plug and **b** the obtained 2D MRI image

phase inside core plug has ^1H magnetic signal, we could calculate the average oil saturation of the core plug by the following approach.

2.3.1 Average Oil Saturation

The NMR compatible core holder is kept stationary so that the MRI imaging area is not offset in multiple measurements during the entire process of flooding. Each pixel of the 2D projection imaging data is viewed as a basic research unit. We denote the magnetic signal amplitude of pixel (x, y) at time t and initial irreducible water state by $SI(x, y, t)$ and $SI(x, y, Swc)$ respectively. Because $SI(x, y, t)$ and $SI(x, y, Swc)$ have nearly the same T1- and T2- weight under the same pulse sequence parameters. The bulk average oil saturation of the core plug at time t in flooding process can be estimated by

$$\bar{S}_o(t) = \frac{\iint SI(x, y, t) \cdot dx dy}{\iint SI(x, y, S_{wc}) \cdot dx dy} \cdot \bar{S}_o(S_{wc}) \quad (1)$$

In Eq. (1), $\bar{S}_o(S_{wc})$ represents the average oil saturation of the core plug in initial irreducible water state and is viewed as prior information, the value can be determined by a volumetric measurement of the effluent water in process of oil saturation and pore volume (PV).

2.3.2 Spatially Solved Displacement Efficiency

By comparing image obtained at time t to initial image, we could eliminate relaxation time weighted effects as much as possible. The displacement efficiency of each pixel at time t is given by

$$\eta(x, y, t) = \frac{SI(x, y, S_{wc}) - SI(x, y, t)}{SI(x, y, S_{wc})} \quad (2)$$

Notably, the displacement efficiency in Eq. (2) is equivalent to the recovery efficiency of the individual pixel units. The displacement efficiency used in this research is the macroscopic displacement efficiency [2], not the displacement efficiency in the microscopic pores. According to Eq. (2), the spatial distribution of the displacement efficiency at different flooding states can be calculated.

2.3.3 Colour Mapping and Statistical Analysis

Colour vision is a fast way for humans to obtain information. A colormap is a mapping from data values to colours that generates visual structures for the data. Colour mapping is a vital method for users to gain insights into the data via a visualization [33]. We employed this technique to mapping the spatial displacement efficiency to colormap by which we could directly show the enhanced oil recovery effect of polymer flooding. Also, we evaluated the improvement in the displacement efficiency and the uniformity in the displacement by analysing the change in the mean and variance of the spatial displacement efficiency before and after polymer flooding.

3 Experiment

3.1 Materials

The core plug used in the NMR experiments was sandstone cut from a sampled core of Xinjiang oilfield, China. The Plug had a porosity $\Phi=21.7\%$, with 1 PV = 8.04 cm³, and a Klinkenberg permeability $k=68.9$ md, with external dimensions 2.41 cm × 8.12 cm (diameter × length). A summary of the sample properties is given in Table 1. Another specimen cut from the same sampled core was prepared for micro-CT scanning with a diameter of 8 mm and a length of 20 mm to make the experimental results more comparable. Crude oil was used as the oil phase at

Table 1 Properties of the rock core used in the NMR flooding experiments

No	Length (cm)	Diameter (cm)	Volume (cm ³)	Porosity (%)	Pore volume (cm ³)	Permeability (md)
21A	8.12	2.41	37.04	21.7	8.04	68.9

26.20 mPa·s at 30 °C. The water phase employed for flooding was a D₂O brine solution with a total dissolved potassium chloride content of 2%, which has no magnetic signal. The KYPAM-2SP polymer (Beijing Hengju Chemical Group Corporation, Beijing, China) was used and diluted to a concentration of 0.2 wt% in the D₂O brine solution. The viscosity of the polymer solution was 109 mPa·s at a shear rate of 7 s⁻¹.

3.2 Equipment

The MRI core flooding system was equipped with a fluid injection system, a displacement system, and an NMR measurement system, as shown in Fig. 3.

The fluid injection system consisted of a Teledyne-ISCO piston pump and three cylinders that contained crude oil, D₂O brine, and polymer solution. The Teledyne-ISCO piston pump was employed for fluid injection into the core plug.

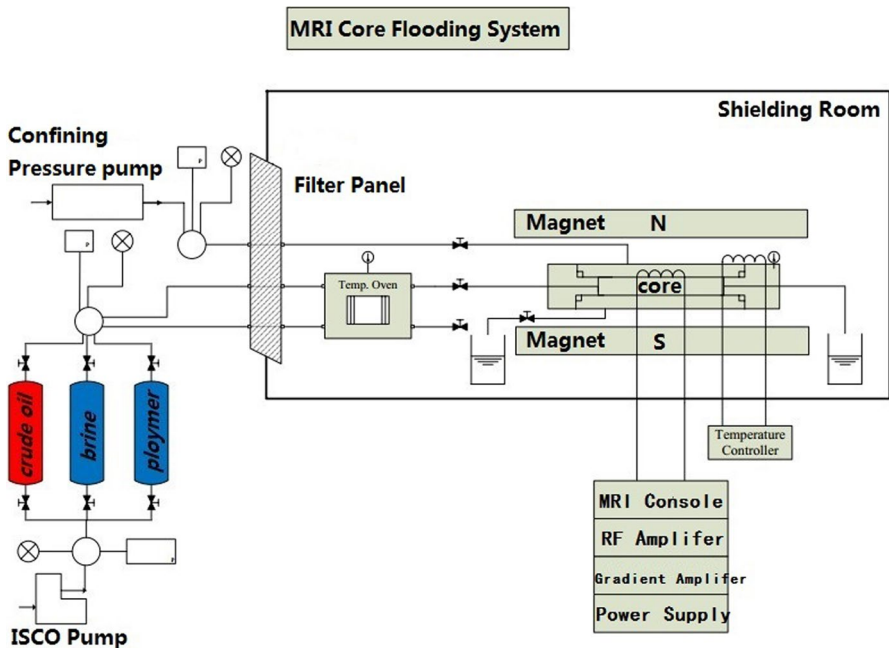


Fig. 3 Schematic of the MRI core flooding system

The displacement system mainly included a homemade NMR compatible core holder and a confining pressure pump. The core holder was made of polyether ether ketone (PEEK) material and was pressurized at a preset confining pressure by the confining pressure system to simulate the in situ formation pressure. Hydrogen-free perfluorocarbon oil was used as a confining fluid.

NMR and MRI measurements were performed on a 0.35 T permanent MRI system with a nonmagnetic core analyser (SPEC-35 Beijing SPEC Technology Development Co., Ltd.) during the flooding process. The MRI measurement system mainly consisted of a spectrometer, an RF amplifier, gradient amplifiers, a coil and a shielding room. The air gap of the magnet was 310 mm, which was large enough for the online core flooding experiments. A coil with an inner diameter of 100 mm was used for excitation and signal detection. The shielding room was implemented to isolate the electromagnetic interference from the flooding equipment outside to improve the SNR and the stability of the measurement.

3.3 Procedure

1. The core plug was cleaned and then dried at 80 °C until the weight of the core was unchanged. The dry weight was determined and kept under vacuum for more than 8 h.
2. The core was saturated with D₂O brine for more than 12 h. The wet weight was determined, and the pore volume was calculated by the difference between the dry weight and wet weight.
3. The core was placed in the core holder. The crude oil contained in the cylinder was pumped into the core plug at a constant rate of 0.1 ml/min until there was no effluent water in the outlet, reaching an irreducible water state. Then, the volume of effluent water was recorded, and the irreducible water saturation (or initial oil saturation) was calculated.
4. D₂O brine flooding was carried out in a constant flow mode of 0.1 ml/min until the water content in the outlet reached 98%. In this process, T₂ distribution and magnetic resonance imaging measurements were carried out.
5. The polymer solution was pumped into the core plug in a constant flow mode of 0.1 ml/min until 0.7 PV had been injected. In this process, T₂ distribution and magnetic resonance imaging measurements were conducted.
6. Another cycle of water flooding was conducted at the same flow rate. The D₂O brine was pumped into the core plug until no oil was produced in the outlet. T₂ distribution and magnetic resonance imaging measurements were also conducted.

The MRI flooding experiment was performed at room temperature and an isotatic confining pressure of 5 MPa. The initial oil saturation, determined by volumetric measurement, was 69.21%. T₂ decay signals and MRI images in different flooding states were obtained by the CPMG and modified SE imaging pulse sequences, respectively. The inversion of T₂ distribution is carried out by homemade software based on BRD method [34]. Table 2 shows the NMR and MRI measurement parameters.

Table 2 Magnetic resonance measurement parameters

CPMG	90° pulse length (μs)	11.5	
	180° pulse length (μs)	23	
	Echo time (μs)	200	
	Repetition delay (s)	3	
	Number of echo	4096	
	Number of averages	8	
	Time consumed (s)	24	
	SE imaging	90° pulse length (μs)	1500
		180° pulse length (μs)	23
		Repetition delay (ms)	300
		Number of averages	4
		Echo time (μs)	3500
		Field of view (mm)	100×100
		Number of image pixels	128×128
Number of slices		1	
Half scan factor	0.6		
Imaging time (s)	93		

Additionally, micro-CT scanning of the smaller specimen by the same flooding procedure as MRI was conducted and the 3D distribution of remaining oil in different displacement stages were reconstructed.

4 Results and Discussion

4.1 Visualization of the Dynamic Flooding Process by MRI

MRI images of the core plug obtained during the dynamic flooding process are shown in Fig. 4. The flow direction of the injectant is from the top to the bottom. Generally, the brighter the area is, the higher the porosity is. The MRI image of the irreducible water state shows that the core plug is highly heterogeneous, which is verified by the mercury injection results and micro-CT image shown in Fig. 5. In the initial water flooding process, the oil recovery is improved with increasing water PV injection, the magnetic signal decreases and the displacement can be clearly observed. After the injection of 1.45 PV, the oil in the core plug is hardly displaced by the water, and the MRI images of 1.45 PV and 3.04 PV are almost the same. The T_2 distribution of these two states also verifies this point. The T_2 distribution contrast in different flooding states is shown in Fig. 6a, and the estimates of bulk oil saturation through the relative size of the T_2 area are shown in Fig. 6b.

Although we have obtained magnetic resonance images of the core during the flooding process, the images are relaxation weighted, and appropriate analysis methods should be established to obtain quantitative information. The signal amplitude of the volume unit is affected not only by oil saturation but also by the corresponding porosity and relaxation of oil. Therefore, it is difficult to determine the spatial

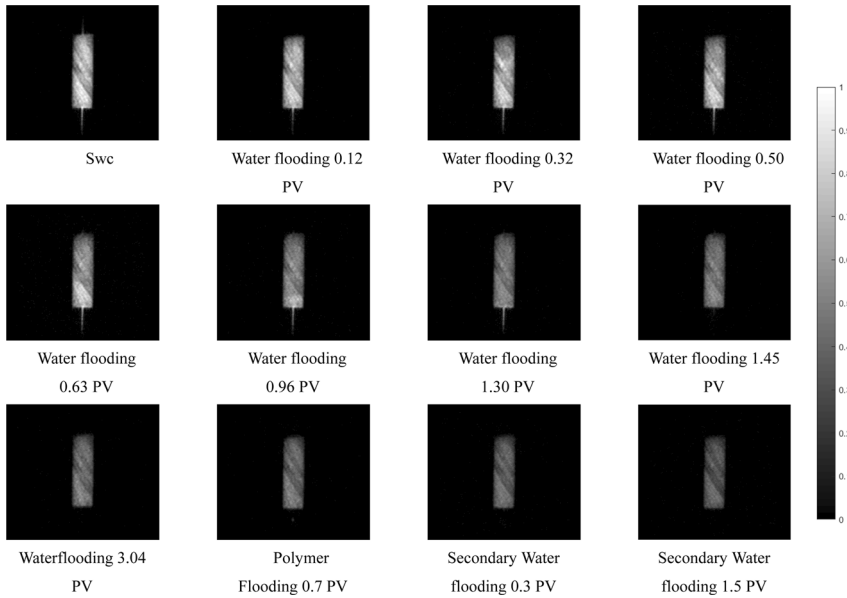


Fig. 4 MRI images of the 21A core during the dynamic flooding process using the modified SE imaging method (the flow direction of the injectant is from the top to the bottom)

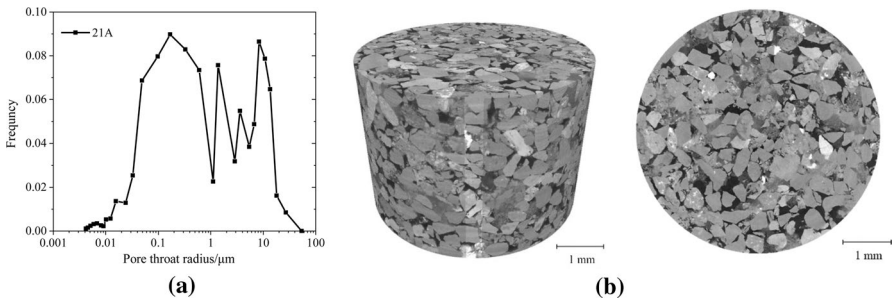


Fig. 5 **a** Pore throat radius distribution of 21A determined by mercury injection; **b** the micro-CT image of the smaller specimen in dry state (spatial resolution is 3.0 μm)

distribution of oil saturation through the SE imaging method. However, we can obtain quantitative information of oil by comparing MRI images to the initial image with the same measurement parameters that provide a calculation basis according to Eq. (1). The quantitative parameters that we obtained are the bulk (average) oil saturation and macroscopic displacement efficiency. To verify the validity of the method, we calculated the bulk oil saturation using the MRI image contrast method and compared it with the bulk oil saturation using the T_2 area method. The results show that the two methods have good consistency, as shown in Fig. 7, and the detailed data are listed in Table 3.

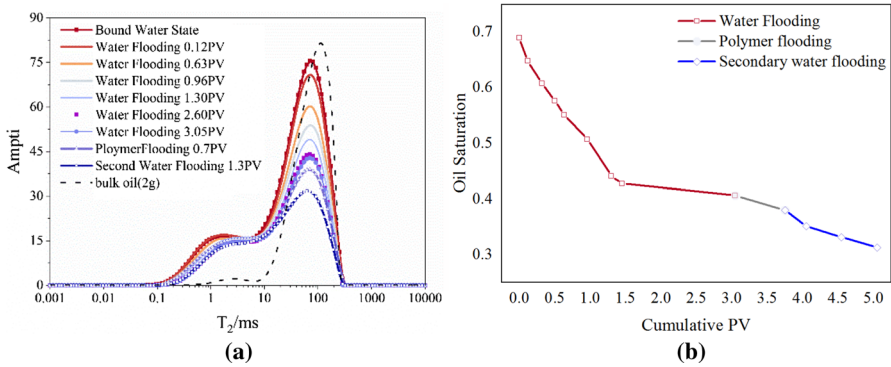
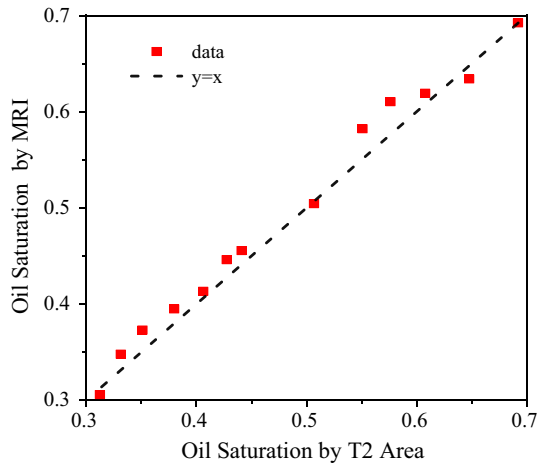


Fig. 6 T2 distribution curves in different flooding states and average oil saturation calculated by the NMR signal amplitude: **a** T2 distribution contrast and **b** decline in the oil saturation during the flooding process

Fig. 7 Average oil saturation determined by the MRI and T2 methods in core plug 21A. The dashed diagonal is the identity line. Good agreement is observed between the two independent estimates of remaining oil saturation



4.2 Spatial Distribution of the Displacement Efficiency

Figure 8 shows the spatial displacement efficiency maps after the initial water flooding and the subsequent polymer flooding (including the secondary water flooding). The colour bar on the right side gives the scale, ranging from 0 to 1. The displacement efficiency in the pipeline at the end of initial water flooding is nearly equal to 1 (shown in red). After polymer flooding, the displacement efficiency was obviously improved. The CT scanning results of the small specimen presented in Fig. 9 give a visual representation of the phenomenon: The grey in the picture represents the rock matrix, the blue represents brine, and the red represents crude oil. After polymer flooding, there was less crude oil remaining in the sample. The displacement efficiency has been increased from 0.2 to 0.5 of the

Table 3 Comparison of the average oil saturation values during the flooding processes from MRI and T2 methods

Flooding process	Cumulative flood volume/PV	\bar{S}_o (T ₂ area method)/%	\bar{S}_o (MRI method)/%
Water flooding	0	69.21	69.21
	0.12	64.78	64.03
	0.32	60.79	61.89
	0.50	57.65	61.03
	0.63	55.11	58.20
	0.96	50.70	50.42
	1.30	44.11	45.55
	1.45	42.76	44.60
	3.05	40.63	41.31
Polymer flooding	3.75	38.00	39.47
Secondary water flooding	4.05	35.11	37.27
	4.55	33.14	34.77
	5.05	31.27	30.27

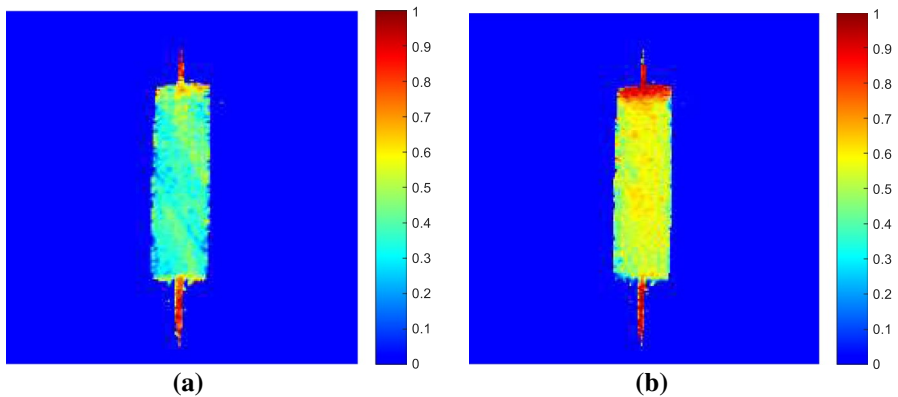


Fig. 8 Comparison of the spatial displacement efficiency **a** after initial water flooding and **b** after subsequent polymer flooding (including secondary water flooding)

initial water flooding to 0.4–0.6. In addition, the inlet region is strongly washed, and the spatial distribution of the displacement efficiency becomes more uniform.

The above results can also be obtained by comparing the histogram of the spatial displacement efficiency after the initial water flooding and subsequent polymer flooding processes, as shown in Fig. 10. The average displacement efficiency after polymer flooding is higher and more uniform than that after water flooding. We also calculated the corresponding mean and standard deviation. The average spatial displacement efficiency after polymer flooding increases from 0.4347 to 0.5279, and the standard deviation decreases from 0.094 to 0.067, which confirms the above conclusion. The colour map of the spatial displacement efficiency

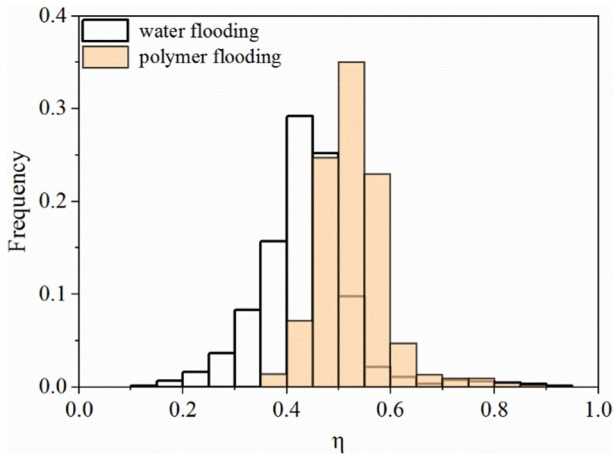


Fig. 9 3D reconstruction of the remaining oil distribution (red colour) in different displacement stages: **a** irreducible water state, **b** after initial water flooding and **c** after subsequent polymer flooding (including secondary water flooding) by micro-CT scanning and image processing [35]

proposed in this paper directly reflects the enhanced oil recovery effect of polymer flooding.

4.3 Displacement Heterogeneity

To study the heterogeneity in the displacement, the core plug was divided into three regions, as shown in Fig. 11. The relative oil saturation reflects the residual level of oil and is defined as the ratio of the oil saturation at some state to the initial oil saturation (\bar{S}_o/\bar{S}_{oi}). The estimates of the relative oil saturation for these target areas in the flooding processes are shown in Fig. 12.

The relative oil saturation as a function of the cumulative injection volume (PV) in the three regions is shown in Fig. 12. In the initial water flooding process (cumulative injection PV is less than 3.05), we can see that region 1 is first flooded, followed by region 2, and finally region 3, which is apparently determined by the spatial location. Before 0.96 PV of the initial water flooding, the oil recovery of region 1 is larger than that of region 2, and region 3 is the lowest, which is mainly affected by the spatial location. The more water injection there is, the more obvious the effect of the water displacement. Afterwards, control by heterogeneity, region 2 is evidently bypassed, the water sweep area is limited, and the relative oil saturation is difficult to further decrease. When 1.30 PV water injection is reached, the relative oil saturation of region 3 is lower than that of region 2 and then quickly synchronizes with region 1. The relative oil saturation decreases slowly in the later water flooding process. At the end of the water flooding (3.05 PV), the residual oil levels of region 1 and region 3 are almost the same, while the relative oil saturation of region 2 is approximately 4% larger. After 0.7 PV of polymer flooding, the oil content of region 1 and region 2 does not obviously change, but the residual oil level of region 3 increases, which is a prominent indication that polymer flooding has come into effect. According to Fig. 12, the polymer flooded

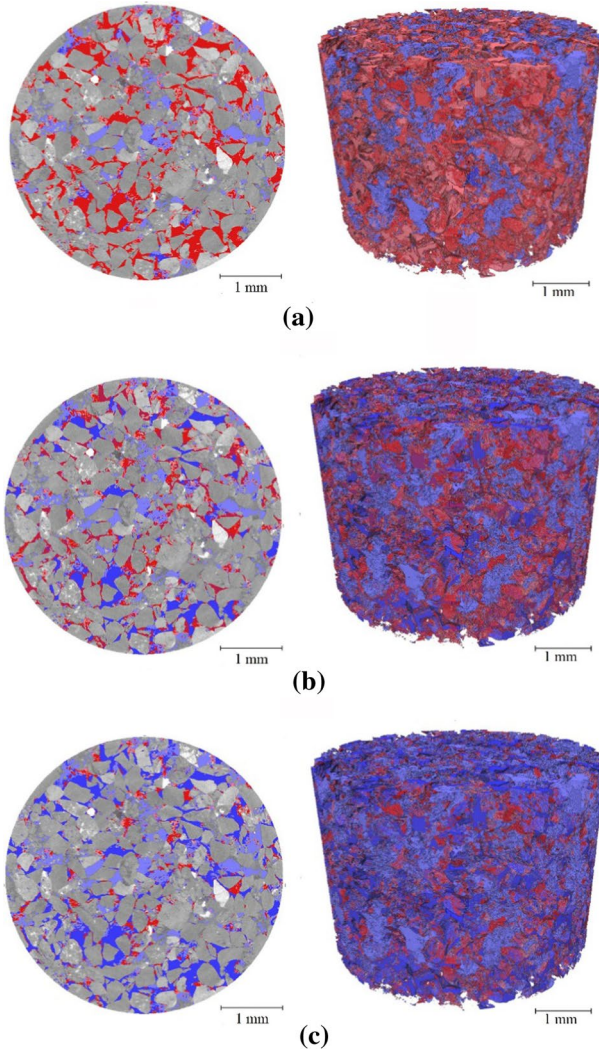


Fig. 10 Compared histogram of the spatial displacement efficiency after initial water flooding and subsequent polymer flooding

the crude oil of region 1 and region 2 into region 3, and the distribution of residual oil clearly changes. In secondary water flooding after polymer injection, the residual oil level in each region decreases rapidly except in region 3, which may be caused by the end effect [6].

Fig. 11 Schematic of the three independent target regions

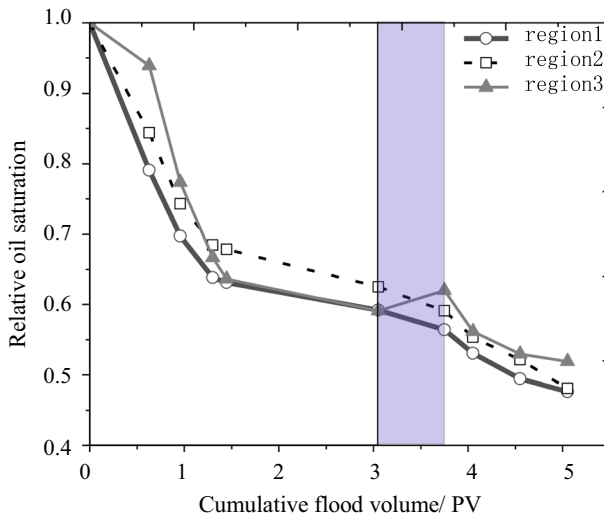
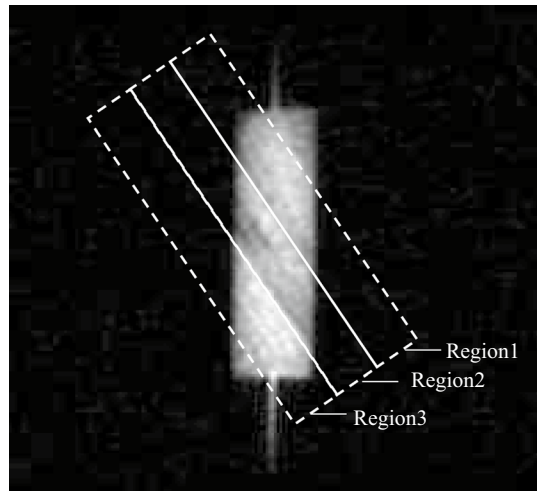


Fig. 12 The changes in the relative oil saturation \bar{S}_o/\bar{S}_{oi} of the three independent regions during flooding. The shaded areas indicate the polymer solution injection process

5 Conclusions

In this paper, we built an MRI/NMR compatible flooding system in a 0.35 T low-field NMR imaging system to carry out a polymer flooding experiment. A modified SE imaging technique was used to achieve fast dynamic 2D MRI imaging of a natural layer core plug. Although the image obtained by the SE method is relaxation weighed, it is a much faster method compared to the pure phase encoding imaging method, which is impractical for studying dynamic flooding. Some quantitative

information, such as the bulk oil saturation and spatial displacement efficiency, are obtained by comparing the MRI images to the initial state with prior information.

The 2D spatial distribution of the displacement efficiency during the flooding process is visualized through a colour mapping technique based on MRI images, and a relevant statistical analysis to determine the change in the mean and variance of the spatial distribution of the displacement efficiency during the flooding process is carried out. The experimental results indicate that the improvement in oil recovery for the natural layered core by polymer flooding after water flooding could be observed very intuitively by the method proposed in this paper. Our MRI methods offer a quantitative approach that will have wide application for flooding mechanism studies of enhanced oil recovery.

Acknowledgements This work was supported by the Key Project of Natural Science Foundation of China (grant numbers 61531002); and the Science Foundation of China University of Petroleum-Beijing at Karamay (grant number No. RCYJ2016B-01-004).

Author Contributions Statement Hongxian Liu: Conceptualization, Methodology, Investigation, Writing—original draft. Yao Ding: Methodology, Investigation, Validation, Writing—original draft. Weimin Wang: Formal analysis, Project administration. Yingkang Ma: Writing—review & editing. Taotao Zhu: Writing—review & editing. Deming Ma: Validation.

Compliance with Ethical Standards

Competing interest The authors declare that they have no known competing financial interests or personal relationships that could have appeared to influence the work reported in this paper.

References

1. R.B. Needham, P.H. Doe, *J. Pet. Technol.* **39**, 1503 (1987)
2. L.W. Lake, *Enhanced Oil Recovery* (Prentice-Hall, Englewood Cliffs, 1989), pp. 314–345
3. D.M. Wang, J.C. Chen, Q.Y. Yang, W.C. Gong, Q. Li, *Acta Pet. Sin.* **21**, 45 (2000)
4. D.M. Wang, J.C. Chen, J.Z. Wu, G. Wang, *Acta Pet. Sin.* **26**, 74 (2005)
5. L.J. Zhang, X.A. Yue, *J. Cent. South Univ. Technol.* **15**, 84 (2008)
6. J. Mitchell, J. Staniland, R. Chassagne, K. Mogensen, S. Frank, E.J. Fordham, *J. Pet. Sci. Eng.* **108**, 14 (2013)
7. J. Mitchell, T.C. Chandrasekera, D.J. Holland, L.F. Gladden, E.J. Fordham, *Phys. Rep.* **526**, 165 (2013)
8. W.M. Wang, H.K. Guo, D.Q. Sun, S.Z. Zhang, *Acta Pet. Sin.* **18**, 54 (1997)
9. N.P. Ramskill, I. Bush, A.J. Sederman, M.D. Mantle, M. Benning, B.C. Anger, M. Appel, L.F. Gladden, *J. Magn. Reson.* **270**, 187 (2016)
10. D.S. Baldygin, S.K. Nobes, Mitra, *Ind. Eng. Chem. Res.* **53**, 13497 (2014)
11. C. Straley, D. Rossini, H. Vinegar, P. Tutunjian, C. Morriss, *Log Anal.* **38**, 84 (1997)
12. G.R. Coates, L.Z. Xiao, M.G. Primmer, *NMR Logging Principles and Applications* (Gulf Publishing Company, Houston, 2000)
13. K.J. Dunn, D.J. Bergman, G.A. LaTorraca, *Nuclear Magnetic Resonance: Petrophysical and Logging Applications* (Elsevier, Pergamon, New York, 2002)
14. J. Mitchell, E.J. Fordham, *Rev. Sci. Instrum.* **85**, 111502 (2014)
15. H.Y. Carr, E.M. Purcell, *Phys. Rev.* **94**, 630 (1954)
16. S. Meiboom, D. Gill, *Rev. Sci. Instrum.* **29**, 688 (1958)
17. M.D. Hürlimann, M. Flaum, L. Venkataramanan, C. Flaum, R. Freedman, G.J. Hirasaki, *Magn. Reson. Imaging* **21**, 305 (2013)

18. Y.Q. Song, L. Venkataramanan, M.D. Hürlimann, M. Flaum, P. Frulla, C. Straley, *J. Magn. Reson.* **154**, 261 (2002)
19. L. Venkataramanan, Y.Q. Song, M.D. Hürlimann, *IEEE Trans. Signal Process.* **50**, 1017 (2002)
20. J. Mitchell, T.C. Chandrasekera, L.F. Gladden, *Prog. Nucl. Magn. Reson. Spectrosc.* **62**, 34 (2012)
21. A. Pop, I. Ardelean, *Cem. Concr. Res.* **77**, 76 (2015)
22. K.R. Brownstein, C.E. Tarr, *Phys. Rev. A.* **19**, 2446 (1979)
23. B. A. Baldwin, W. S. Yamanashi, *SPE Reserv. Eng.* **4**, 207(1989)
24. C.E. Muir, B.J. Balcom, *Annu. Reports NMR Spectrosc.* **77**, 81 (2012)
25. Q. Chen, F.R. Rack, B.J. Balcom, *Geol. Soc. Spec. Publ.* **267**, 193 (2006)
26. O.V. Petrov, B.J. Balcom, *J Magn Reson.* **212**, 102 (2011)
27. D. Xiao, B.J. Balcom, *J Magn Reson.* **220**, 70 (2012)
28. W.P. Weglarz, A. Krzyzak, M. Stefaniuk, *Magn. Reson. Imaging* **34**, 492 (2016)
29. M. Li, D. Xiao, L. Romero-Zerón, F. Marica, B. MacMillan, B.J. Balcom, *J. Magn. Reson.* **269**, 13 (2016)
30. L.A. Weisenberger, J.L. Koenig, *Macromolecules* **23**, 2445 (1990)
31. D.A. Feinberg, J.D. Hale, J.C. Watts, L. Kaufman, A. Mark, *Radiology* **161**, 527 (1986)
32. J.R. MacFall, N.J. Pelc, R.M. Vavrek, *Magn. Reson. Imaging* **6**, 143 (1988)
33. L. Zhou, C.D. Hansen, *IEEE Trans. Vis. Comput. Graph.* **22**, 2051 (2016)
34. J.P. Butler, J.A. Reeds, S.V. Dawson, *SIAM J. Numer. Anal.* **18**, 381 (1981)
35. J. Hou, Z. Li, S. Zhang, X. Cao, Q. Du, X. Song, *Transp. Porous Media* **79**, 407 (2009)

Publisher's Note Springer Nature remains neutral with regard to jurisdictional claims in published maps and institutional affiliations.